Wind Energy Department
2007

Aerodynamics and Characteristics of a Spinner Anemometer

T F Pedersen[1], N Sørensen[1,2] and P Enevoldsen[3,4]

1 Wind Energy Department, Risø National Laboratory DTU, 4000 Roskilde Denmark
2 Department of Civil Engineering, Aalborg University, 9000 Aalborg Denmark
3 Siemens Wind Power, Brande Denmark

Doi: dx.doi.org/10.1088/1742-6596/75/1/012018

Aerodynamics and Characteristics of a Spinner Anemometer

T F Pedersen[1], N Sørensen[1,2] and P Enevoldsen[3,4]

[1] Wind Energy Department, Risø National Laboratory DTU, 4000 Roskilde Denmark
[2] Department of Civil Engineering, Aalborg University, 9000 Aalborg Denmark
[3] Siemens Wind Power, Brande Denmark

E-mail: troels.friis.pedersen@risoe.dk

Abstract. A spinner anemometer is a wind measurement concept in which measurements of wind speed in the flow over a wind turbine spinner is used for determination of the free wind. Analogies to the concept are the flow around a sphere and a five hole pitot-tube. But, in stead of measuring pressure differences on the surface, the spinner anemometer measures directional air speeds in the flow above the spinner surface. A spinner anemometer, based on a modified 300kW wind turbine spinner, was mounted with three 1D sonic wind speed sensors. The flow around the spinner was calculated with the EllipSys3D CFD-code. Calculations were made for varying wind speeds and yaw angles, and the air speed within the sonic sensor path was determined during rotation. The calculated air speeds were used as "calibration" data for an analogue spinner anemometer algorithm. The algorithm converts, by inclusion of a measured rotor position, the measured sonic sensor air speeds to free wind speed, wind direction relative to the spinner and flow inclination angle. A wind tunnel concept test and a full scale field experiment with a comparison to a 3D sonic anemometer were made. The results indicate that the 300kW spinner anemometer characteristics are comparable to the 3D sonic anemometer with respect to time traces and average and standard deviation of wind speeds.

1. Introduction

A spinner anemometer is a wind measurement concept intended for horizontal axis wind turbines [1]. The spinner anemometer integrates the spinner, which is the aerodynamically formed glass-fibre cover over the rotor hub, with active wind sensors on the spinner into the wind measurement concept. The concept is best explained by an analogy to the five hole pitot-tube or pressure sphere anemometer. But in stead of measuring pressure differences as on the five hole pitot-tube, the spinner anemometer measures directional flow speeds in the flow above the spinner surface, and above the spinner boundary layer.

[4] Acknowledgments to Siemens Wind Power Systems for construction, building and provision of the 300kW modified spinner and tripod support for the experiments and analysis.

2. Description of a spinner anemometer

The shape of a spinner nose on most wind turbines is spherical and similar to the nose of a five hole pitot-tube or a pressure-sphere anemometer, though the size of a spinner is somewhat larger. A pressure-sphere anemometer nose is spherical [2][3]. The spinner anemometer presented here also has a spherical nose, but it has a transition to a cone rather than to a cylinder as for the five hole pitot-tube. One way to measure the wind speed on a wind turbine spinner could therefore be to measure the pressure differences from five holes in the spinner. There are some disadvantages of this, though. One is the sensitivity to rotation, and the other is the sensitivity of pressure tabs to rain and icing.

2.1. Principles of a spinner anemometer

A better sensing method is to measure directional air speed over the spinner, and to use sonic anemometry, which is a conventional and robust measurement principle [4]. A spinner anemometer can thus typically consist of three 1D sonic wind speed sensors, mounted symmetrically at the front of the spinner, as shown in Figure 1. The sonic sensors are mounted with the sensor paths in plane with the rotor axis and with the sonic paths tilted somewhat backwards to allow wind to come undisturbed into the sensor paths and to avoid the sensor head shadow effect [4]. In this way, the wind component on the sensors due to rotation is cancelled out, and only the wind along the axis direction is measured. The tilted-back configuration of the 1D sonic sensor also allows the sensor to be sufficiently narrow to be mounted from the inside of the spinner through a hole in the mounting fitting on the spinner.

The physical principle of the spinner anemometer is based on the air flow over the spinner, see Figure 2. The air flow from the right with an inflow angle of 10º is accelerates from zero at the stagnation point to an air speed above the free wind speed on the upper side of the spinner. On the lower side the air flow accelerates less. This systematic variation of air speed over the spinner with variation of inflow angle is used in reverse to determine the flow angles.

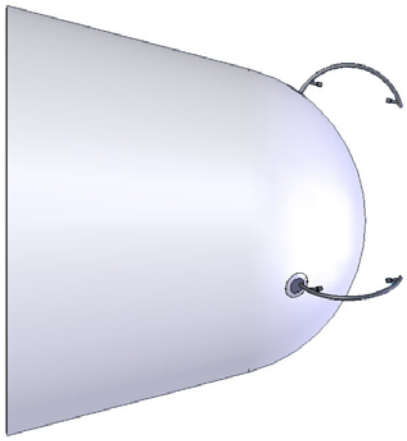

Figure 1 A spinner anemometer with three 1D sonic sensors mounted on the front part of the S300 spinner.

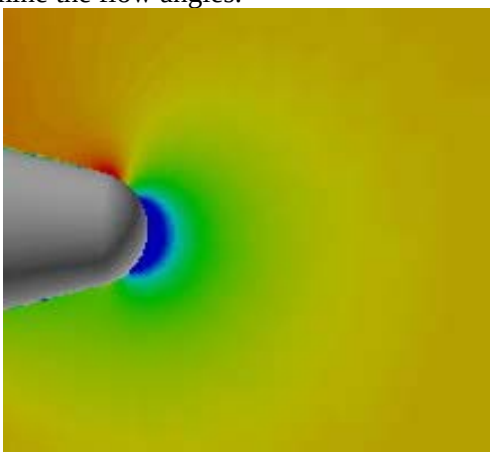

Figure 2 Axial wind speed contours around a rotational symmetric spinner. Wind is from the right and the air inflow angle is 10º from below.

2.2. A spinner anemometer for theoretical and experimental investigations

The specific S300 spinner anemometer shown in Figure 1 is used for theoretical and experimental investigations. The spinner length is 0.92m and the diameter at the back of the spinner is 1.10m. The spinner nose has a radius of 0.40m. The 1D sonic sensors and electronics are based on ordinary 3D sonic sensor technology, but the sensors themselves are specifically designed and built for spinner anemometry. The sensor path lengths are 0.162m, and the sensor path angle to the rotor axis is 11º. Two different types of sonic sensors were used, both having the same supporting geometry, but with

different types of sensor heads. The "classic" sonic sensors have sensor head diameters of 20mm, , while the "new" sonic sensors have sensor head diameters of 12mm. Rotational speed is 15rpm.

3. Wind tunnel concept tests

A test of the measurement concept was made in a large 4x4 m^2 wind tunnel. The S300 spinner was mounted horizontally on a shaft on a tripod. The tripod was mounted on a turn-table in the floor which could be yawed to change angle of attach of the wind on the spinner. A cup anemometer was mounted at the lower left corner of the inlet to the test section. Unfortunately, this was close to a contraction wedge on the floor, that locally increase outlet wind speed, see Figure 3.

Figure 3 Concept tests in a 4x4 m^2 wind tunnel. The spinner is yawed to -90º and the "classic" sonic sensors can be seen on the nose. The cup anemometer is seen in the lower left corner of the inlet (encircled).

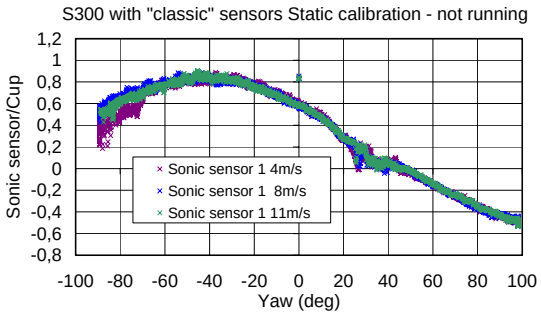

Figure 4 Measurements of "classic" sonic sensor wind speed in horizontal position without rotation and with yaw sweeps from 90º to -90º relative to cup anemometer wind speed at three different wind speeds.

At first, measurements were made without rotation in order to measure the basic flow characteristics. The spinner was positioned so that one sonic sensor was horizontal for the static test. Figure 4 shows the sensor wind speed relative to the cup wind speed, measured at continuous yaw sweeps and at three different tunnel wind speeds for the "classic" type of sonic sensors. Figure 5 and 6 show measurements during rotation with the "classic" type of sensors at 20º and 10º yaw and a wind speed of 9m/s. Index c indicates data have had an "internal" calibration. This means that all data of sensor 1, 2 and 3 have been sorted individually according to ascending values, and sensors 2 and 3 have been regressed on sensor 1. This "internal" calibration is possible because all sensors statistically measure the same wind. In this way the influence of imperfections of spinner, sensors and sensor mounting can be minimized.

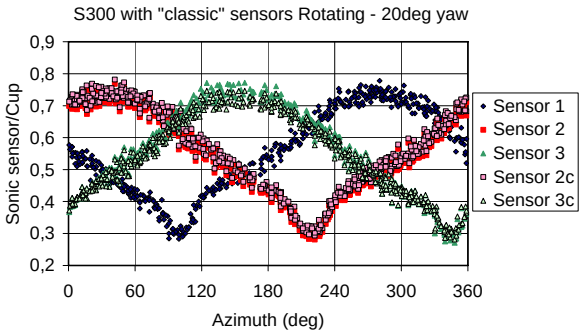

Figure 5 Scatter of measurements of 1D sonic sensor wind speeds relative to cup anemometer wind speed during rotation at a yaw angle of 20º and with "classic" sensor heads.

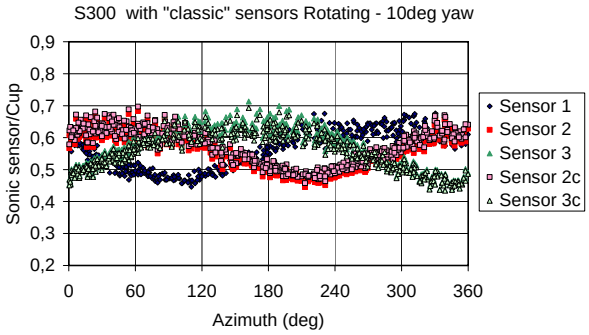

Figure 6 Scatter of measurements of 1D sonic sensor wind speeds relative to cup anemometer wind speed during rotation at a yaw angle of 10º and with "classic" sensor heads.

4. Aerodynamics of a spinner anemometer

The aerodynamics of the S300 spinner anemometer was investigated by a detailed CFD analysis.

4.1. CFD calculations on the S300 spinner

The in-house flow solver EllipSys3D is used in all computations presented in the following. The code is developed in co-operation between the Department of Mechanical Engineering at DTU and The Department of Wind Energy at Risø National Laboratory, see [5], [6] and [7].

The EllipSys3D code is a multiblock finite volume discretization of the incompressible Reynolds Averaged Navier-Stokes (RANS) equations in general curvilinear coordinates, and is second order accurate in space and time. The code uses a collocated variable arrangement, and Rhie/Chow interpolation [8] is used to avoid odd/even pressure decoupling. As the code solves the incompressible flow equations, no equation of state exists for the pressure, and in the present work the SIMPLE algorithm of [9] is used to enforce the pressure/velocity coupling. The EllipSys3D code is parallelized with MPI for executions on distributed memory machines, using a non-overlapping domain decomposition technique. In the present work the turbulence in the boundary layer is modeled by the k-ω SST eddy viscosity model [10].

4.1.1. Computational grid

When modeling the spinner in the computations, the geometry was as shown in Figure 1 and 7. In contrast with the measurements in the tunnel, the support structure for the spinner was not included, and the base of the spinner was modeled as a closed surface. Additionally, only the spinner was modeled, and the flow speeds in the sonic sensor paths were calculated. No attempts were made to include the sonic anemometer geometry in the calculations.

Before the computations can be performed, a computational mesh is needed. For the present computations, the geometry of the spinner was given as a solid body in the form of an IGS file, see Figure 7. Based on the IGS files, the commercial GridGen mesh generation code, were used to generate the surface mesh on the cube.

Finally, the 3D volume mesh was generated using the inhouse Risø enhanced hyperbolic mesh generator HypGrid3D. For the S300 spinner, 256 cells are used around the spinner in the cross stream direction, and 64 cells in the flow direction, and two additional square blocks of 64x64 cells are placed at the nose and rear of the spinner respectively. The number of cells in the normal direction is 64, giving a total cell count of approximately 1.6 million cells. The cells are stretched towards the surface in the normal direction, to assure that the y+ value is below 2. To avoid influence of location of the outer boundary, the boundary is located more than 10 diameters away from the spinner.

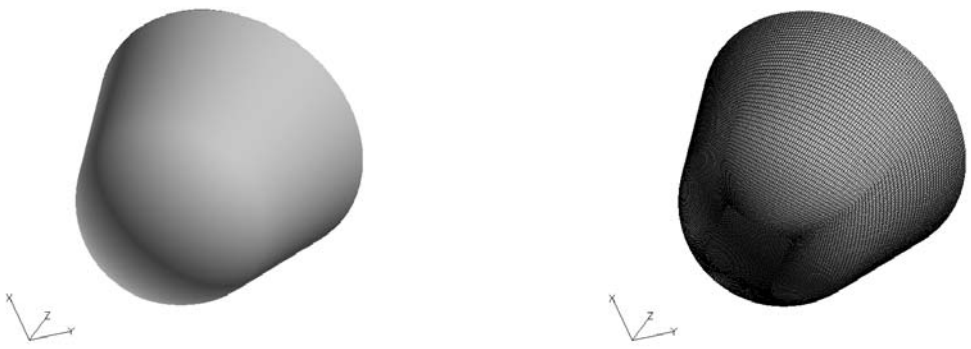

Figure 7 Perspective view of S300 spinner left and the surface mesh generated on the geometry right.

4.1.2. Influence of wind speed

In the original wind tunnel setup, the 'free stream' velocity was measured with a cup anemometer placed near the floor at the entrance of the tunnel. Due to local flow distortion by the contraction wedge on the floor, the velocity measured by the cup anemometer was not representative for the actual speed in the test region of the tunnel. To investigate this phenomenon a series of computations were performed for the 10º and 20º yaw settings for varying wind speeds. These computations showed that good agreement with the measured values by the cup anemometer of 9 m/s could be obtained by adjusting the free wind speed to 6.5 m/s for the 20º degrees case, see Figure 9. For the 10 º yaw case an adjustment to 7.5 m/s was made as shown in Figure 8. These findings indicate that the cup measurements were influenced by the local flow distortion, and that the tunnel blocking was influenced by the presence of the spinner. Afterwards, the experiment in free wind confirmed that the change in wind speed predicted by the CFD computations agree well with the actual behavior of the flow near the spinner.

Besides establishing the actual flow velocity in the test section, it could be seen from the computations with varying inflow velocity that it is possible to directly scale the velocity to obtain the same good agreement as by adjusting the inflow velocity. This can be seen as a proof that the main effect of the spinner can be represented by an inviscid flow assumption.

4.1.3. Influence of rotation

To investigate the effect of the spinner rotation on the flow field, comparison of computations with zero and a finite rotational speed corresponding to 15 RPM for 0º, 10º and 20º yaw cases were performed, see Table 1. From Figure 9 it can be seen that the rotation of the spinner, has a very weak influence on the measured velocity profiles, and can easily be ignored for practical purpose. Even though the results do not show any dependence of the spinner rotation, we still include the spinner rotation when computing the velocity characteristics at different yaw angles, as the additional computational overhead is unimportant.

Table 1 The operational conditions for the s300 spinner used in the computations.

Yaw Angle [deg]	Velocity [m/s]	RPM
0	10	0
0	10	15
10	7.5	0
10	7.5	15
10	8	0
10	10	0
10	10	15
20	6.5	0
20	10	0
20	10	15
30	10	15
40	10	15
60	10	15
80	10	15

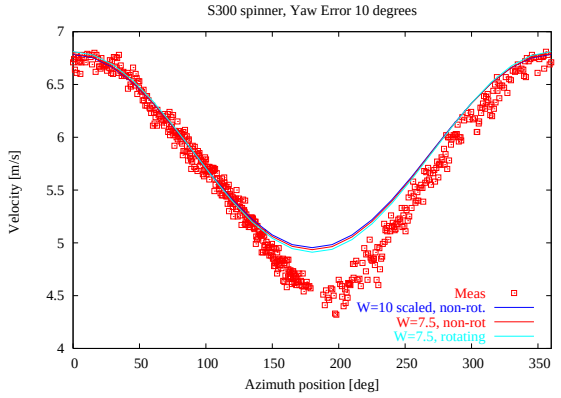

Figure 8 Comparison of the computed and measured velocity distribution around the S300 spinner. The W=10 [m/s] curve is scaled with a factor 0.75.

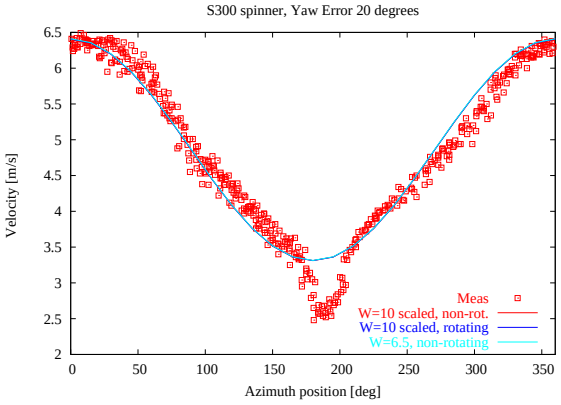

Figure 9 Comparison of the computed and measured velocity distribution around the S300 spinner for the 20 degrees yaw case. The W=10 [m/s] curve is scaled with a factor 0.65.

4.1.4. Deviation from the measurements

Due to the physical design of the sonic sensors, flow from some directions will be distorted by the supporting structure and the sensor heads see the measurements in Figure 9. In the computations, the sensors are not modeled, and the computations thus do not include any distortion of the flow by the sonic sensor itself. Looking at Figure 9 for the 20º yaw situation, there is observed a region with large deviations by a narrow gap between measured and computed velocities. This is due to the sensor head shadow effect. A similar observation is not made for the 10º yaw situation shown in Figure 8, if the wind is scaled to the same factor as in Figure 9.

4.1.5. Variation of the velocity signal with yaw setting

Having verified that the CFD method is capable of predicting the correct behavior of the flow around the spinner, when excluding the sensor head shadow effect, a series of computations for different yaw settings were performed, see Table 1. Here we use a wind speed of 10 m/s, as the previous computations has shown that the curves can easily be scaled to fit other wind speeds. The azimuth behaviour of the velocity signal as function of the yaw settings of the spinner can be seen in Figure 10, where the behaviour is shown for yaw setting of 0 º, 10 º, 20 º, 30 º, 40 º, 60 º and 80º.

The calculated average wind speeds in the sonic sensor paths are seen to be very close to sinus shaped, and they appear to be of a family of curves that reduce the average sensor wind speed over one rotation with increasing yaw setting angle while the amplitude increases. In fact the average sensor wind speed is reduced with the cosine to the yaw setting angle while the amplitude increases with the sine. The signal of one sonic sensor can thus be expressed as a function of the flow angle α and the azimuth position φ, the free wind speed U, and two constants K_1 and K_2:

$$V_S = U(K_1 \cos\alpha + K_2 \sin\alpha \cos\varphi) \qquad (1)$$

With this expression for one sensor we can now express the air speed for the three sensors positioned symmetrically on the spherical nose:

$$V_{S1} = U(K_1 \cos\alpha + K_2 \sin\alpha \cos\varphi) \qquad (2)$$

$$V_{S2} = U(K_1 \cos\alpha + K_2 \sin\alpha \cos(\varphi + 2\pi/3)) \qquad (3)$$

$$V_{S3} = U(K_1 \cos\alpha + K_2 \sin\alpha \cos(\varphi + 4\pi/3)) \qquad (4)$$

The inverse problem, where the sensor path air speeds are known, and the wind conditions are to be determined, has a simple solution. The three expressions of air speed for the sensor paths have three unknowns, the azimuth angle φ of the stagnation point on the spinner, the flow angle of the stagnation

point to the rotor axis α, and the free wind speed U. The azimuth angle is expressed by one out of three formulations as:

$$\varphi = Ar\tan\frac{\sqrt{3}(V_{S2}-V_{S3})}{V_{S2}+V_{S3}-2V_{S1}} \qquad (5)$$

The flow angle to the rotor axis is expressed by one out of three formulations as:

$$\alpha = Ar\tan\frac{K_1(V_{S2}-V_{S1})}{K_2(V_{S1}\cos(\varphi+2\pi/3)-V_{S2}\cos\varphi)} \qquad (6)$$

And the wind speed as:

$$U = (V_{S1}+V_{S2}+V_{S3})/(3K_1\cos\alpha) \qquad (7)$$

The azimuth angle φ depend on the three airspeeds alone, and is independent of the constants K_1 and K_2. The wind speed is proportional to the average of the three sensor wind speeds, and is only dependent on the flow angle to the rotor axis α. These equations are reasonably simple to apply for an algorithm of the spinner anemometer. The CFD calculated values are compared to the sonic sensor expression (2) in Figure 10. They compare extremely well up to 60º. Only at 80º the function values deviate from the CFD calculations.

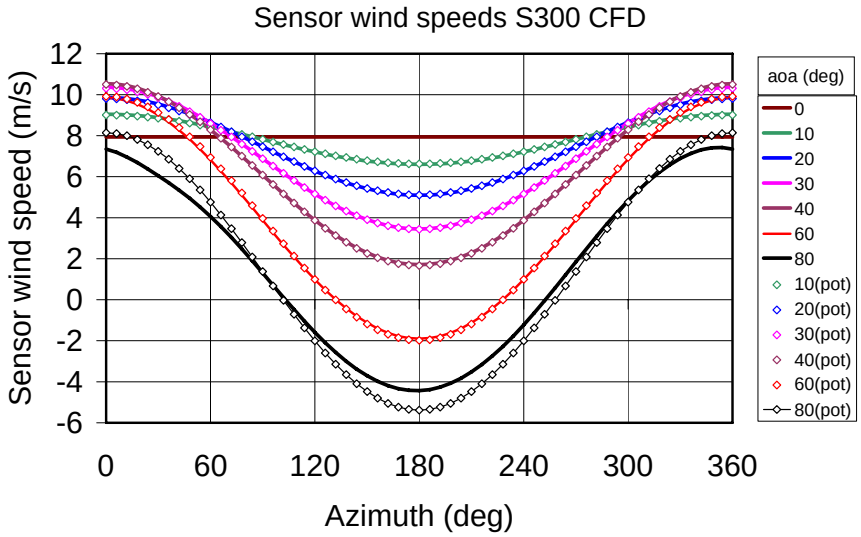

Figure 10 The computed velocity distribution around the S300 spinner for the 0º, 10º, 20º, 30º, 40º, 60º, 80º yaw case (the velocities are not scaled), and the values from formula (2).

5. Free field comparison to 3D sonic anemometer

The S300 spinner anemometer was tested under field conditions at the Risø test site. In this case only the "new" sensors were used in order to reduce the sensor head shadow effect.

5.1. Free field experimental setup

A 3D Gill Windmaster sonic anemometer was mounted with the sensor heads at same height and about three meters to the side and a little in front of the spinner anemometer for comparison tests. Measurements were made while rotating at 15rpm. The whole arrangement of the spinner and sonic sensors are shown in Figure 11.

5.2. Comparison of spinner anemometer with 3D sonic anemometer

100 seconds time traces of the two wind sensors are shown in Figure 12, 13 and 14. Figure 12 shows comparison of scalar winds, while Figure 13 shows the yaw angle, and Figure 14 the flow inclination angle. The measured wind speeds and wind directions by the two anemometers seem to follow each other quite well. The most significant variations are the same for the two sensors. The 10min average absolute wind speed of the 3D sonic is only 2% lower than the spinner anemometer wind speed for the time trace, of which is shown 100secs in Figure 12. Figure 15 and 16 show compared average wind speeds and standard deviations over a 3 hour measurement period. Average values have a slope of 0.975, and the standard deviations 1.045.

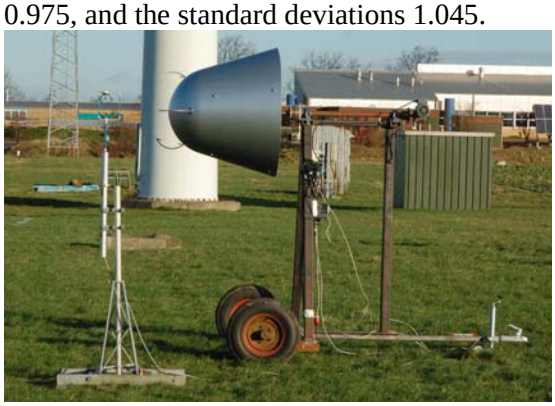

Figure 11 Arrangement of the S300 spinner anemometer with "new" sensors in comparison with the sonic anemometer at Risø test site

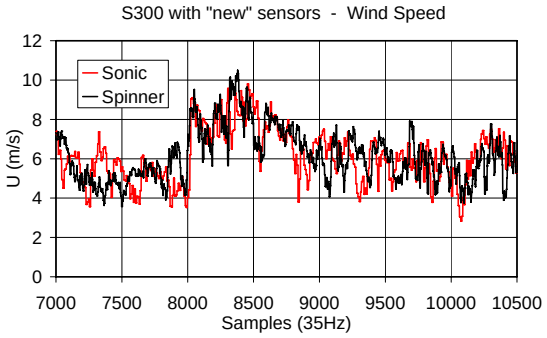

Figure 12 Comparison of measured wind speed at 35Hz sampling rate (100sec of data) of spinner anemometer and 3D sonic anemometer

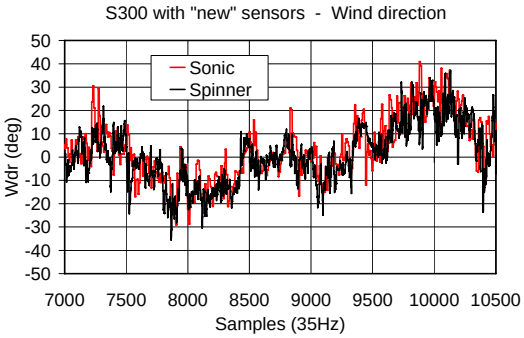

Figure 13 Comparison of measured horizontal inflow angle at 35Hz sampling rate

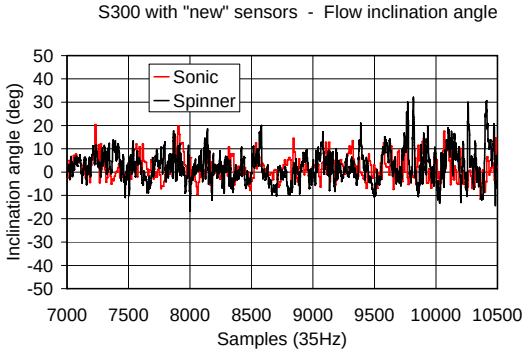

Figure 14 Comparison of measured vertical inflow angle at 35Hz sampling rate

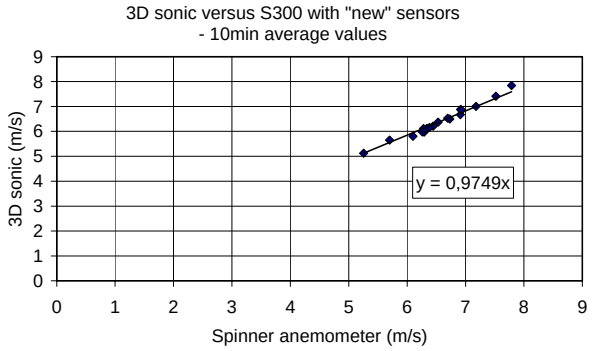

Figure 15 10min average wind speed values

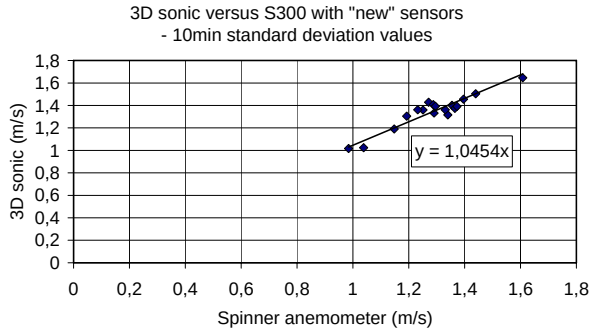

Figure 16 10min stddev wind speed data

6. Conclusions

A 300kW wind turbine spinner anemometer has been investigated by wind tunnel tests, field tests, and by theoretical CFD calculations. Two types of sonic sensors were tested with 20mm "classic" and 12mm "new" sensor head diameters, respectively. The wind tunnel tests revealed that the "classic" sensor heads did have flow distortion that gave a wind speed drop gap for azimuth positions when the flow is parallel to the sonic sensor paths.

A full CFD analysis of the spinner anemometer was made. The results showed that the calculations were almost insensitive to rotation and to wind speeds. For all flow or yaw angles up to 60º the azimuth variation was a pure cosine. At 80º there was a significant deviation from the cosine form. The shape of the responses of the sonic sensors to a flow or yaw angle can be described with a simple function that over one revolution decreases the average value with a cosine to the flow angle and increases the amplitude with a sine to the flow angle. The function can be described for all three sonic sensors, and from the equations, the wind speed, the flow angle to the rotor axis and the azimuth position on the spinner can be determined and be used in a conversion algorithm for the spinner anemometer.

Field measurements were made with the spinner anemometer and the "new" sonic sensors with reduced sensor head shadow effect. The conversion algorithm was used, and no sensor head corrections were applied. The spinner anemometer was compared to a standard 3D sonic anemometer, and the results showed that the time traces of the two instruments follow quite well, considering the distance between the two instruments and the low level of 2.5m above the ground. Over a period of three hours, the average values of the spinner anemometer were 2.5% higher than the sonic anemometer, and the standard deviation values were 4.5% lower.

References

[1] Pedersen T F, Sørensen N N, Madsen H A, Courtney M, Møller R, Enevoldsen P and Egedal P 2007 Spinner anemometry - an innovative wind measurement concept, *Proc. EWEC 2007 Milan 7-10 May 2007 (preprint)*

[2] Thurtell, G.W., Tanner, C.B., Wesely, M.L., 1970, Three-Dimensional Pressure-Sphere Anemometer System, *Journal of Applied Meteorology Volume 9 pp 379-385*

[3] Wesely, M.L., Tanner, C.B., 1972, An Improved Pressure-Sphere Anemometer, *Boundary Layer Meteorology pp 275-283*

[4] Cuerva A, Sanz-Andrés A, Franschini S, Eecen P, Busche P, Pedersen TF, Mouzakis F, "ACCUWIND, Accurate Wind Measurements in Wind Energy, Task 2, Improve the Accuracy of Sonic Anemometers", EU-FP6 project report, June 2006

[5] Michelsen, J.A.. Basis3D - a Platform for Development of Multiblock PDE Solvers. Technical Report AFM 92-05, Technical University of Denmark, 1992.

[6] Michelsen J.A., ”Block structured Multigrid solution of 2D and 3D elliptic PDE's”, Technical Report AFM 94-06, Technical University of Denmark, 1994.

[7] Sørensen, N.N.. General Purpose Flow Solver Applied to Flow over Hills. Risø-R- 827-(EN), Risø National Laboratory, Roskilde, Denmark, June 1995.

[8] Rhie C.M. ”A numerical study of the flow past an isolated airfoil with separation” Ph.D. thesis, Univ. of Illinois, Urbane-Champaign, 1981.

[9] Patankar S.V. and Spalding D.B. ”A Calculation Procedure for Heat, Mass and Momentum Transfer in Three-Dimensional Parabolic Flows.” Int. J. Heat Mass Transfer, 15:1787,1972

[10] Menter F.R., ”Zonal Two Equation k-ω Turbulence Models for Aerodyanmic Flows”. AIAA-paper-932906, 1993.